Discover Nano

Discover

Research

Properties and alcohol sensing applications of quasi-2D $(PEA)_2(MA)_3Sb_2Br_9$ thin films

Chien-Min Hun[1] · **Lung-Chien Chen**[1]

Received: 2 November 2022 / Accepted: 16 February 2023

Abstract

We fabricated an alcohol detector based on $(PEA)_2(CH_3NH_3)_3Sb_2Br_9$ ($(PEA)_2MA_3Sb_2Br_9$) lead-free perovskite-like films. The XRD pattern revealed that the $(PEA)_2MA_3Sb_2Br_9$ lead-free perovskite-like films exhibited a quasi-2D structure. The optimal current response ratios are 74 and 84 for 5 and 15% alcohol solutions, respectively. When the amount of PEABr decreases in the films, the conductivity of the sample in ambient alcohol with a high alcohol concentration solution increases. The alcohol was dissolved into water and carbon dioxide due to the catalyst effect of the quasi-2D $(PEA)_2MA_3Sb_2Br_9$ thin film. The rise and fall times for the alcohol detector were 1.85 and 0.7 s, respectively, indicating that the detector was suitable.

Keywords Lead-free perovskite · $(PEA)_2MA_3Sb_2Br_9$ · Quasi-2D material · Alcohol detectors

Abbreviations

QTD	Quasi-two-dimensional
$(PEA)_2(MA)_3Sb_2Br_9$	Palmitoylethanolamide methylammonium antinomy bromide
$SbBr_3$	Antimony tribromide
MABr	Methylammonium bromide
DMF	Dimethylformamide
PEABr	Phenethylamine hydrobromide
FESEM	Field-emission scanning electron microscopy
ITO	Indium tin oxide

Introduction

Organic–inorganic lead halide $MAPbX_3$ ($MA = CH_3NH_3$, X = Cl, Br, and I) perovskite is widely used in solar cells, light-emitting diodes (LEDs), detectors, and lasers. Due to its excellent optoelectronic properties in exciton binding energy, carrier mobility, carrier diffusion lengths, light absorption range, and tunable optical band gap by using composition variation, perovskite is suitable for the solar spectrum. Therefore, perovskite solar cells have quickly attracted widespread attention in the field of high-efficiency photovoltaic cells [1–10]. For the past decade, the power conversion efficiency

✉ Lung-Chien Chen, ocean@ntut.edu.tw; Chien-Min Hun, dreamsmin@gmail.com | [1]Department of Electro-Optical Engineering, National Taipei University of Technology, Taipei 10608, Taiwan.

of perovskite solar cells has rapidly increased from less than 5% to 25.7% [11–14]. Although the efficiency has been significantly improved, due to the considerable influence of the environment on the efficiency of the device, such as the humidity in the ambient air, the stability of the device cannot be significantly improved for a long time [15–17].

The perovskite materials also applied in gas sensing field owing to their fascinating catalytic property caused by a lot of defects and oxygen vacancies [18, 19]. In addition, the toxicity of lead-based perovskites may also be a major obstacle for sensor applications. The lead toxicity problem of perovskite gas sensors is more important than that of solar cells and LEDs because the gas sensor film needs to be exposed to air for a long time and because of the environmental impact on the sensor performance. Recently, a lead (Pb)-free material with the similar structure as perovskite has emerged: $A_3B_2X_9$ (A = MA or Cs; B = Bi or Sb; X = I, Br, and Cl). The bismuth and antimony halide materials are typical perovskite-like material with no toxicity, such that they are potential materials for optoelectronic and biochemical applications [20–24]. Since Bi is a low-toxicity element adjacent to Pb, $A_3Bi_2X_9$, which has better stability than $MAPbI_3$ perovskite [24], can be used as a substitute for Pb-based perovskite materials. Thus, it is a potential new light absorbing material. As an element belonging to the same main group as Bi, Sb has a similar arrangement and distribution of outer electrons to Bi and has been used as a substitute material for Pb [25].

However, to our knowledge, these low-toxicity perovskite materials have not been investigated in the field of gas sensors. Considering that this type of material can solve the aforementioned problems, after exploring related materials, we demonstrate for the first time a new application of lead-free perovskite $(PEA)_2MA_3Sb_2Br_9$ in alcohol (C_2H_5OH) detection. Compared with the use of MA^+, the introduction of PEA^+ enhances the hydrophobicity and stability of perovskite materials [26–28]. In this study, the performance and results show that the $(PEA)_2MA_3Sb_2Br_9$ alcohol detector exhibits relatively excellent performance.

Experiments

Sensor Manufacturing Process

The precursors $SbBr_3$, MABr, and PEABr were dissolved in 1 mL of DMF and stirred at RT for 30 min at 750 rpm to obtain $(PEA)_2MA_3Sb_2Br_9$ perovskite solutions. The structure of $(PEA)_2MA_3Sb_2Br_9$ is shown in Fig. 1a. The recipe is listed in Table 1. A total of 50 µL of the prepared perovskite solution was dropped on glass with an ITO pattern, and a two-stage spin coating was performed using a spin coater. The first stage was 1000 rpm for 10 s, and the second stage was 5000 rpm for 20 s to form perovskite films. Additionally, 100 µL of toluene was dropped on the surface and then baked on a hot plate at 100 °C for 10 min.

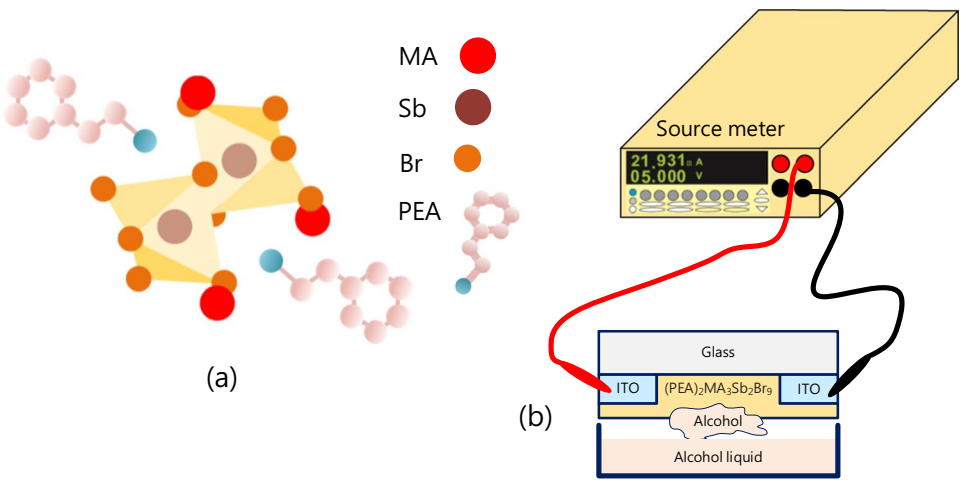

Fig. 1 **a** Structure of $(PEA)_2MA_3Sb_2Br_9$ and **b** sketch of the experimental set up

Table 1 Recipe of various $(PEA)_2MA_3Sb_2Br_9$ films

Sample	$SbBr_3$ (mmol/ml)	MABr (mmol/ml)	PEABr (mmol/ml)
PEA1	1	0.8	0.4
PEA2	1	0.9	0.2
PEA3	1	0.975	0.05
$MA_3Sb_2Br_9$	1	1	0

Measurement

The $(PEA)_2MA_3Sb_2Br_9$ perovskite sensor was placed in air, and a voltage from 0 to 10 V was applied to record the background current. After that, the $(PEA)_2MA_3Sb_2Br_9$ sensor was placed in an alcohol environment, and after waiting for 30 s, a voltage of 0 to 10 V was applied again, and its current–voltage (*I*–*V*) characteristics were recorded. Figure 1b sketches the experimental set up. In alcohol response measurement, the definition of the normalized responsivity ratio (R) of the sensor is as follows:

$$R = \frac{\Delta I}{I_0} = \frac{(I - I_0)}{I_0} \tag{1}$$

where I_o is the background current and I is the signal current under ambient alcohol at 10 V. To observe the different sensitivities of the sensor to alcohol during a period of time, we measured the current–time (*I*–*T*) characteristics of the $(PEA)_2MA_3Sb_2Br_9$ alcohol sensors. The applied voltage is 10 V. The first step is to put the sensor in the air, and after 30 s, we put the sensor in an alcohol environment. The study of optical properties in this work includes photoluminescence (PL) and absorbance spectra using a HITACHI F-7000 spectrophotometer.

Results and discussion

Figure 2a shows the samples with various $(PEA)_2MA_3Sb_2Br_9$ films. More amount of $MA_3Sb_2Br_9$ is present in the film, and more the sample look yellowish due to the MaBr band gap of 2.34 eV [29]. According to these SEM images, we noticed that with more PEABr, the surface morphology is rougher, as shown in Fig. 2b–d. For the cross-sectional SEM images, there are some holes on the surface of the PEA1 film, as show in Fig. 3a. However, as shown in Fig. 3b, c, for the samples of PEA2 and PEA3, layer-by-layer stacked 2D films without holes were observed.

To investigate the formation of $(PEA)_2MA_3Sb_2Br_9$ films, we performed grazing incidence X-ray diffraction (XRD) with wavelength of 1.54 Å. Figure 4 presents the XRD patterns for PEA1, PEA2, PEA3, and $MA_3Sb_2Br_9$ films. In the XRD patterns, it can be indexed to trigonal symmetry with space group P3m1, and five peaks were observed. They are 6.1°, 6.7°, 8.7°, 17.7°, and 26.7°, respectively, corresponding to the (030) and (10-1) phases of PEABr and the (001), (002), and (003) phases of $MA_3Sb_2Br_9$. The first two peaks of the XRD peaks are the 2D structure of PEABr [29–31].

The crystallinity and defect level in perovskite films can be observed by photoluminescence (PL). The PL emission spectra of the $(PEA)_2MA_3Sb_2Br_9$ films with different amounts of PEABr are shown in Fig. 5a. There is one PL emission peak for all samples. The peak positions for PEA1, PEA2, PEA3, and $MA_3Sb_2Br_9$ are 420, 430, 465, and 524 nm, respectively. A sharp absorption edge was observed, as shown in Fig. 5b. The absorption positions of the PEA1, PEA2, PEA3, and $MA_3Sb_2Br_9$ films are 420 nm, 440 nm, 470 nm, and 520 nm, respectively. They correspond to the energy gap. To calculate the band gap according to the PL and absorption spectra, the band gap is 3.02, 2.88, and 2.66 eV for samples of PEA1, PEA2, and PEA3, respectively, as shown in Fig. 6. The layer numbers are 1, 2, and 3 [30].

Figure 7a shows the current–voltage (*I*–*V*) characteristics for PEA1, PEA2, and PEA3 samples in the ambient 5% alcohol concentration. We measured the *I*–*V* curves and estimated the current response ratio, as shown in Fig. 7b. All samples on the ambient alcohol with an alcohol concentration of 5% showed the highest current response ratio. For the PEA2 and PEA3 samples, as the alcohol concentration in the solution increases, the current response ratio still increases. This may be due to the dissolution of alcohol water and carbon dioxide induced by the catalyst effect of the quasi-2D

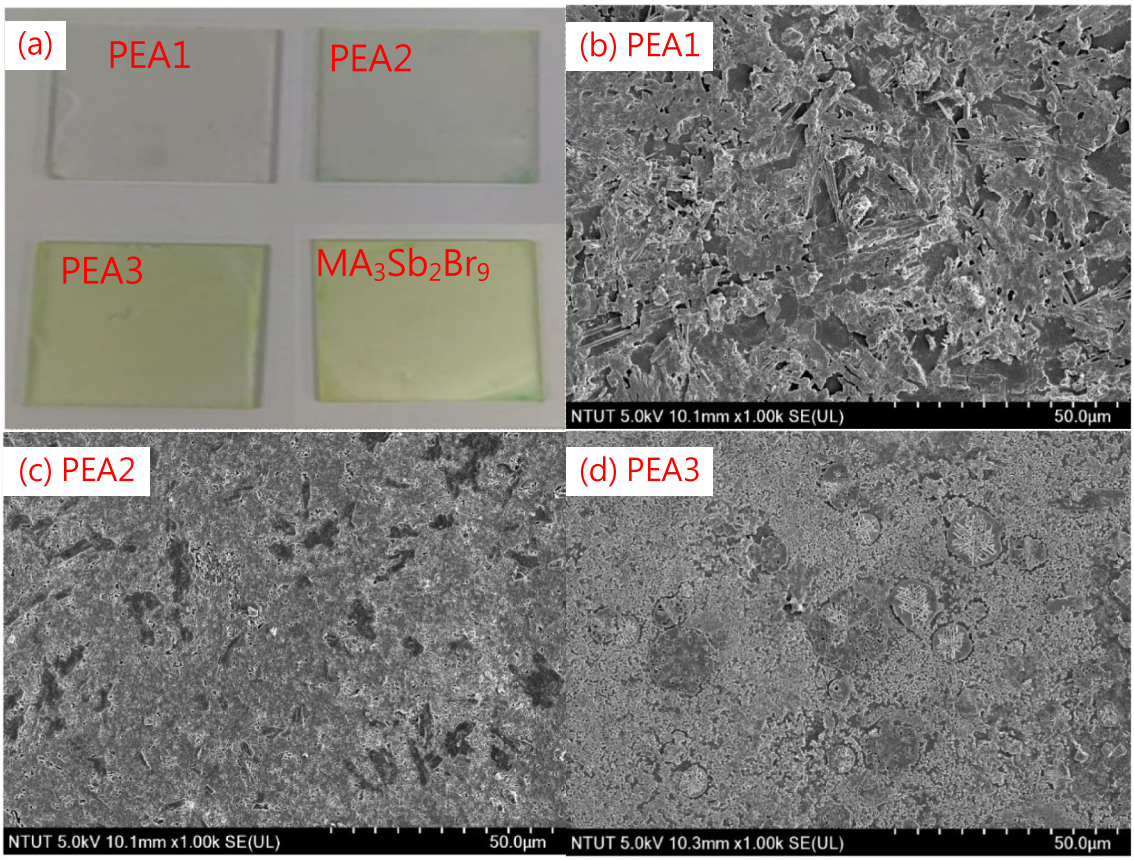

Fig. 2 Pictures and top-view SEM images of $(PEA)_2MA_3Sb_2Br_9$ films with different amounts of PEABr

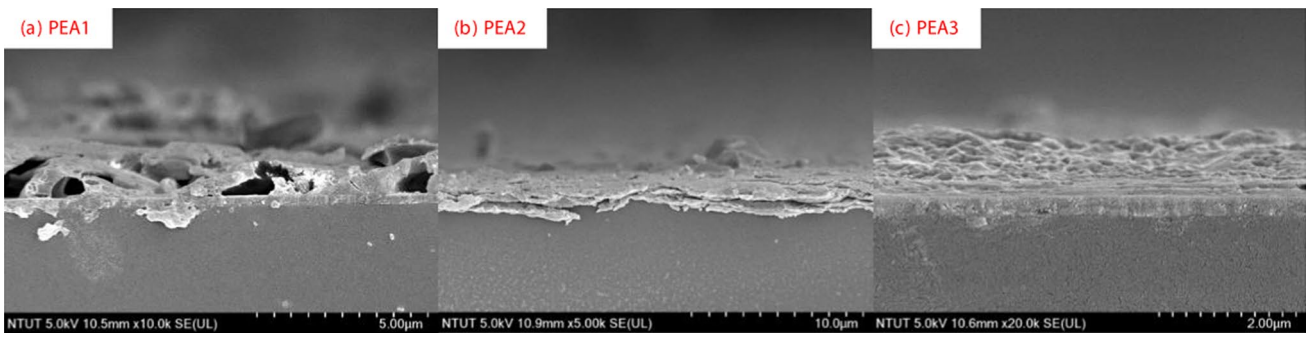

Fig. 3 Cross-sectional SEM images of $(PEA)_2MA_3Sb_2Br_9$ films with different amounts of PEABr

$(PEA)_2(MA)_3Sb_2Br_9$ thin film. Figure 8 shows the current response of the $(PEA)_2MA_3Sb_2Br_9$ thin-film alcohol sensors with different PEABr compositions. The rise and fall times of the PEA3 alcohol detectors were 1.85 and 0.7 s, respectively, which were faster than the rise time (3.1 and 3.7 s) and fall times (5.4 and 3.2 s) of the PEA1 and PEA2 alcohol detectors, respectively. This indicates better conductivity and fewer surface states.

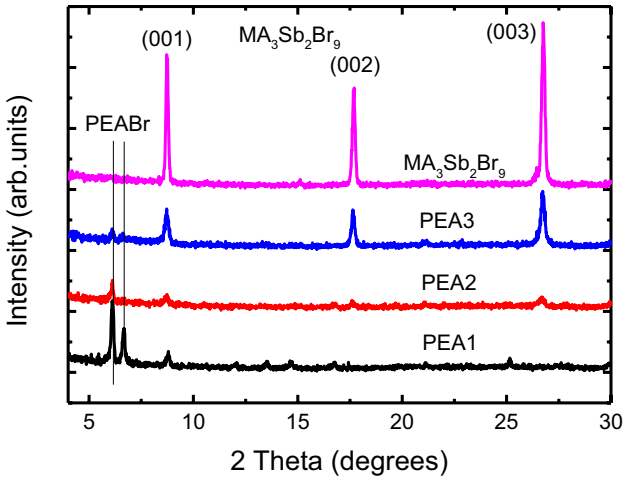

Fig. 4 XRD patterns of the PEA1, PEA2, PEA3, and $MA_3Sb_2Br_9$ films

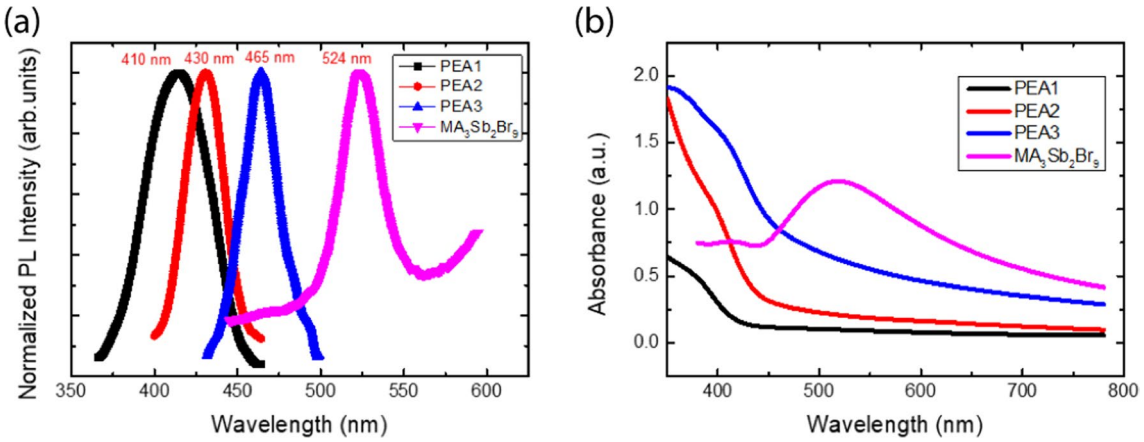

Fig. 5 **a** Photoluminescence spectra (PL) and **b** absorption spectra of $(PEA)_2MA_3Sb_2Br_9$ films with different amounts of PEABr and $MA_3Sb_2Br_3$ film

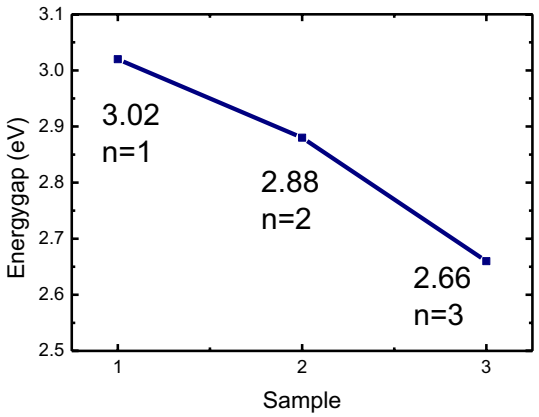

Fig. 6 Bandgap of $(PEA)_2MA_3Sb_2Br_9$ films with different numbers of layers, n

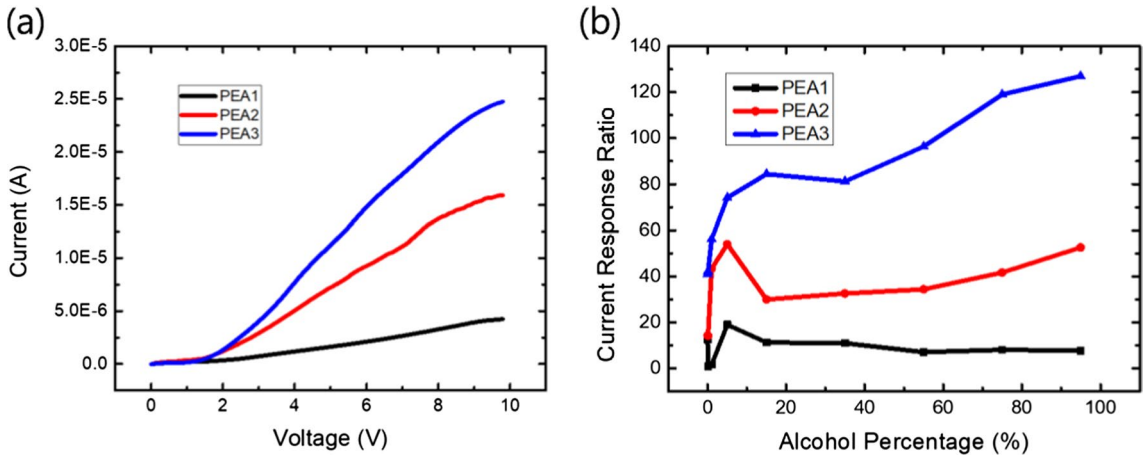

Fig. 7 **a** Current–voltage characteristics and **b** current response ratio of $(PEA)_2MA_3Sb_2Br_9$ films with different alcohol concentrations

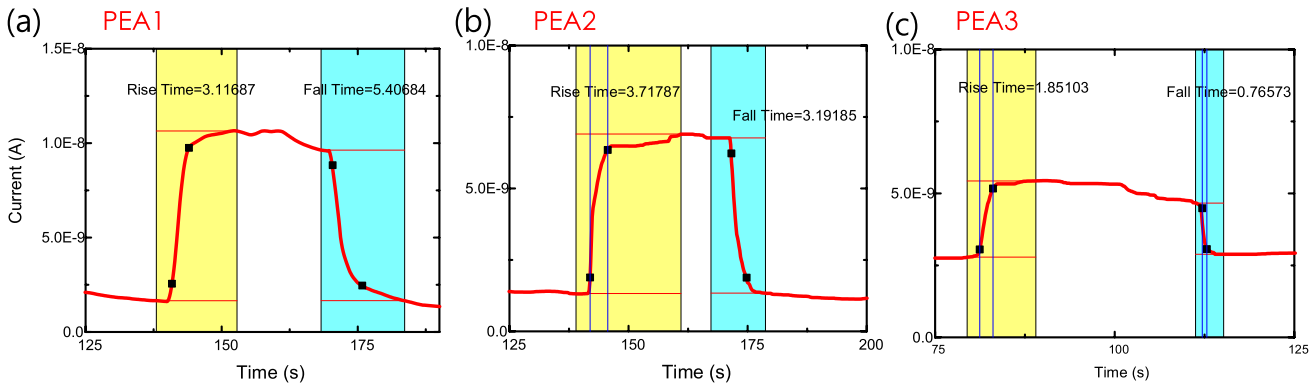

Fig. 8 Current response of the $(PEA)_2MA_3Sb_2Br_9$ thin film alcohol detectors with different PEABr compositions: **a** PEA1: 0.4 mmol/ml, **b** PEA2: 0.2 mmol/ml, and **c** PEA3: 0.05 mmol/ml

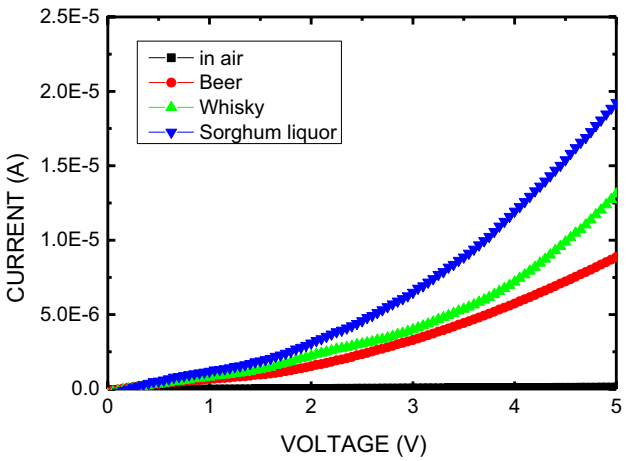

Fig. 9 Current–voltage characteristics of PEA3 sample in various alcoholic beverage ambient

Finally, for real application, real sample characteristics using commercially available alcoholic beverage have presented in Fig. 9 to clarify the suitability of this work. The alcohol by volumes (ABV) of beer, whisky, and sorghum liquor are 5, 40, and 58%, respectively. As shown in Fig. 9, when the ABV increases, the resistance decreases. The current response ratio of beer,

whisky, and sorghum liquor are 69, 103, and 152, respectively, for PEA3 sample. It may be contributed to the conductivity of the $(PEA)_2MA_3Sb_2Br_9$ film. Therefore, this work is suitable for the application of industry.

Conclusions

In conclusion, we have studied the characteristics of $(PEA)_2MA_3Sb_2Br_9$ thin films and their application to alcohol detectors. The optimal current response ratios are 74 and 84 for 5 and 15% alcohol solutions, respectively. When the amount of PEABr decreases in the films, the conductivity of the sample in ambient alcohol with a high alcohol concentration solution increases. This may be due to the dissolution of alcohol into water and carbon dioxide induced by the catalyst effect of the quasi-2D $(PEA)_2(MA)_3Sb_2Br_9$ thin film. The situation in which the conductivity of the sample increased under ambient alcohol with increasing alcohol concentration in solution improved.

Acknowledgements This work was supported by the National Science and Technology Council of Taiwan (No. 111-2221-E-027-040-MY3).

Author contributions L-CC: Conceptualization, Analysis, Writing – review & editing. C-MH: Methodology, Sample preparation, and measurement. All authors reviewed the manuscript. Both authors read and approved the final manuscript.

Funding Ministry of Science and Technology under Contract Nos. 111-2221-E-027-040-MY3.

Data availability All the data are fully available without restrictions.

Declarations

Ethics approval and consent to participate All authors agreed on the ethics approval and consent to participate.

Consent for publication Not applicable.

Competing interests The authors declare no competing interests.

References

1. Liu C, Cheng YB, Ge Z. Understanding of perovskite crystal growth and film formation in scalable deposition processes. Chem Soc Rev. 2020;49:1653–87.
2. Liu XK, Xu W, Bai S, Jin Y, Wang J, Friend RH, Gao F. Metal halide perovskites for light-emitting diodes. Nat Mater. 2020;20:1–12.
3. Wang Y, Song L, Chen Y, Huang W. Emerging new-generation photodetectors based on low-dimensional halide perovskites. ACS Photonics. 2019;7:10–28.
4. Dong H, Zhang C, Liu X, Yao J, Zhao YS. Materials chemistry and engineering in metal halide perovskite lasers. Chem Soc Rev. 2020;49:951–82.
5. Stoeckel M, Gobbi M, Bonacchi S, Liscio F, Ferlauto L, Orgiu E, Samorì P. Reversible, fast, and wide-range oxygen sensor based on nanostructured organometal halide perovskite. Adv Mater. 2017;29:1702469.
6. Lee JW, Seol DJ, Cho AN, Park NG. High-efficiency perovskite solar cells based on the black polymorph of $HC(NH_2)_2PbI_3$. Adv Mater. 2014;26:4991–8.
7. Saliba M, Correa-Baena JP, Graetzel M, Hagfeldt A, Abate A. Perovskite solar cells: from the atomic level to film quality and device performance. Angew Chem Int Ed. 2018;57:2554–69.
8. Stranks SD, Eperon GE, Grancini G, Menelaou C, Alcocer MJ, Leijtens T, Herz LM, Petrozza A, Snaith HJ. Electron hole diffusion lengths exceeding 1 micrometer in an organometal trihalide perovskite absorber. Science. 2013;342:341–4.
9. Li F, Zhang C, Huang J, Fan H, Wang H, Wang P, Zhan C, Liu CM, Li X, Yang LM, Song Y, Jiang KJ. A cation-exchange approach for the fabrication of efficient methylammonium tin iodide perovskite solar cells. Angew Chem Int Ed. 2019;58:6688–92.
10. Yao F, Peng J, Li R, Li W, Gui P, Li B, Liu C, Tao C, Lin Q, Fang G. Room-temperature liquid diffused separation induced crystallization for high-quality perovskite single crystals. Nat Commun. 2020;11:1–9.

11. Kojima A, Teshima K, Shirai Y, Miyasaka T. Organometal halide perovskites as visible-light sensitizers for photovoltaic cells. J Am Chem Soc. 2009;131:6050–1.
12. Yao J, Qiu B, Zhang ZG, Xue L, Wang R, Zhang C, Chen S, Zhou Q, Sun C, Yang C, Xiao M, Meng L, Li Y. Cathode engineering with perylene-diimide interlayer enabling over 17% efficiency single-junction organic solar cells. Nat Commun. 2020;11:1–10.
13. Chen LC, Tien CH, Lee KL, Kao YT. Efficiency improvement of $MAPbI_3$ perovskite solar cells based on a $CsPbBr_3$ quantum dot/Au nanoparticle composite plasmonic light-harvesting layer. Energies. 2020;13:1471.
14. National Renewable Energy Laboratory. Best research-cell efficiencies. https://www.nrel.gov/pv/assets/pdfs/best-research-cell-efficiencies-rev220630.pdf. Accessed 30 June 2022.
15. Sharma SK, Phadnis C, Das TK, Kumar A, Kavaipatti B, Chowdhury A, Yella A. Reversible dimensionality tuning of hybrid perovskites with humidity: visualization and application to stable solar cells. Chem Mater. 2019;31:3111–7.
16. Mosconi E, Azpiroz JM, De Angelis F. Ab initio molecular dynamics simulations of methylammonium lead iodide perovskite degradation by water. Chem Mater. 2015;27:4885–92.
17. Nickel NH, Lang F, Brus VV, Shargaieva O, Rappich J. Unraveling the lightinduced degradation mechanisms of $CH_3NH_3PbI_3$ perovskite films. Adv Electron Mater. 2017;3:1700158.
18. Maity A, Raychaudhuri AK, Ghosh B. High sensitivity NH_3 gas sensor with electrical readout made on paper with perovskite halide as sensor material. Sci Rep. 2019;9:7777.
19. Fergus JW. Perovskite oxides for semiconductor-based gas sensors. Sens Actuators B Chem. 2007;123:1169–79.
20. Ahmad K, Ansari SN, Natarajan K, Mobin SM. A $(CH_3NH_3)_3Bi_2I_9$ perovskite based on a two-step deposition method: lead-free, highly stable, and with enhanced photovoltaic performance. Chem Electro Chem. 2019;6:1192–8.
21. Ahmad K, Kumar P, Mobin SM. A two-step modified sequential deposition method-based Pb-free $(CH_3NH_3)_3Sb_2I_9$ perovskite with improved open circuit voltage and performance. Chem Electro Chem. 2020;7:946–50.
22. Kumar P, Ahmad K, Dagar J, Unger E, Mobin SM. Two-step deposition approach for lead free $(NH_4)_3Sb_2I_9$ perovskite solar cells with enhanced open circuit voltage and performance. Chem Electro Chem. 2021;8:3150–4.
23. Ahmad K, Mobin SM. Organic-inorganic copper(II)-based perovskites: a benign approach toward low-toxicity and water-stable light absorbers for photovoltaic applications. Energy Techno. 2019;8:1901185.
24. Park BW, Philippe B, Zhang X, Rensmo H, Boschloo G, Johansson EMJ. Bismuth based hybrid perovskites $A_3Bi_2I_9$ (A: methylammonium or cesium) for solar cell application. Adv Mater. 2015;27:6806–13.
25. Ahmad K, Mobin SM. Recent progress and challenges in $A_3Sb_2X_9$-based perovskite solar cells. ACS Omega. 2020;5:28404–12.
26. Liao Y, Liu H, Zhou W, Yang D, Shang Y, Shi Z, Li B, Jiang X, Zhang L, Quan LN, Quintero-Bermudez R, Sutherland BR, Mi Q, Sargent EH, Ning Z. Highly oriented low-dimensional tin halide perovskites with enhanced stability and photovoltaic performance. J Am Chem Soc. 2017;139:6693–9.
27. Ghasemi M, Lyu M, Roknuzzaman M, Yun JH, Hao M, He D, Bai Y, Chen P, Bernhardt PV, Ostrikov K, Wang L. Phenethylammonium bismuth halides: from single crystals to bulky-organic cation promoted thin-film deposition for potential optoelectronic applications. J Mater Chem A. 2019;7:20733–41.
28. Cheng B, Li TY, Wei PC, Yin J, Ho KT, Retamal JRD, Mohammed OF, He JH. Layer-edge device of two-dimensional hybrid perovskites. Nat Commun. 2018;9:5196.
29. Hun CM, Tien CH, Lee KL, Lai HY, Chen LC. The effects of temperature on the growth of a lead-free perovskite-like $(CH_3NH_3)_3Sb_2Br_9$ single crystal for an MSM photodetector application. Sensors. 2021;21:4475.
30. Li Z, Chen Z, Yang Y, Xue Q, Yip HL, Cao Y. Modulation of recombination zone position for quasi-two-dimensional blue perovskite light-emitting diodes with efficiency exceeding 5%. Nat Commun. 2019;10:1027.
31. Xing J, Zhao Y, Askerka M, Quan LN, Gong X, Zhao W, Zhao J, Tan H, Long G, Gao L, Yang Z, Voznyy O, Tang J, Lu ZH, Xiong Q, Sargent EH. Color-stable highly luminescent sky-blue perovskite light-emitting diodes. Nat Commun. 2018;9:3541.